

# Dielectrophoresis of nanocolloids: a molecular dynamics study

E. Salonen<sup>1,a</sup>, E. Terama<sup>1,b</sup>, I. Vattulainen<sup>1,2,c</sup>, and M. Karttunen<sup>3,d</sup>

<sup>1</sup> Biological Physics and Soft Matter Group, Laboratory of Physics and Helsinki Institute of Physics, Helsinki University of Technology, P.O. Box 1100, FI-02015 HUT, Finland

<sup>2</sup> Memphys-Center of Biomembrane Physics, Physics Department, University of Southern Denmark, DK-5230 Odense M, Denmark

<sup>3</sup> Biophysics and Statistical Mechanics Group, Laboratory of Computational Engineering, Helsinki University of Technology, P.O. Box 9203, FI-02015 HUT, Finland

Received: November 9, 2004 / Revised version: September 4, 2018

**Abstract.** Dielectrophoresis (DEP), the motion of polarizable particles in non-uniform electric fields, has become an important tool for the transport, separation, and characterization of microparticles in biomedical and nanoelectronics research. In this article we present, to our knowledge, the first molecular dynamics simulations of DEP of nanometer-sized colloidal particles. We introduce a simplified model for polarizable nanoparticles, consisting of a large charged macroion and oppositely charged microions, in an explicit solvent. The model is then used to study DEP motion of the particle at different combinations of temperature and electric field strength. In accord with linear response theory, the particle drift velocities are shown to be proportional to the DEP force. Analysis of the colloid DEP mobility shows a clear time dependence, demonstrating the variation of friction under non-equilibrium. The time dependence of the mobility further results in an apparent weak variation of the DEP displacements with temperature.

**PACS.** 82.20.Wt Computational modeling; simulation – 61.25.Hq Macromolecular and polymer solutions; polymer melts; swelling – 82.70.Dd Colloids

## 1 Introduction

A polarizable particle in a non-uniform electric field is set in motion due to the coupling between the electric field gradient and the induced polarization. This effect was named *dielectrophoresis* (DEP) by Pohl in his pioneering studies in the 1950's [1,2]. DEP can be understood by considering the simple picture of a dipole in a non-uniform electric field. The dipole will be at least partly oriented in the direction of the field gradient and hence one end of the dipole will experience a stronger electric field strength than the other. This results in a non-zero net force and the dipole is set in motion.

If the polarizable particle is smaller than the characteristic length at which the electric field  $\mathbf{E}$  changes appreciably, the DEP force affecting the particle can be approximated as a coupling between its induced dipole moment  $\mathbf{p}$  and the field,

$$\mathbf{F}_{\text{DEP}} = (\mathbf{p} \cdot \nabla) \mathbf{E}. \quad (1)$$

For an ideal dielectric the induced dipole moment is linearly proportional to the electric field,  $\mathbf{p} = \alpha_p \mathbf{E}$ , where  $\alpha_p$  is the

total effective polarizability of the particle that depends on the dielectric properties of the particle and the suspending medium. Combining this relation with Eq. (1), one obtains a general equation for the DEP force,

$$\mathbf{F}_{\text{DEP}} = \frac{1}{2} \alpha_p \nabla E^2. \quad (2)$$

Two important observations can be made from Eq. (2). First, the direction of the DEP force is parallel to the gradient of the electric field squared, but does not depend on the actual polarity of the field. Hence, the same DEP effect can be achieved with both DC and AC electric fields. Second, the direction of the force also depends on the polarizability of the particle. If the particle is more polarizable than the medium, it will be attracted to regions of higher field strength. If, on the other hand, the particle is less polarizable, it will be repelled from the high-field regions. The first case is commonly referred to as *positive* DEP and the latter as *negative* DEP.

With modern microfabrication techniques based on photo- and electronlithographies it is possible to routinely manufacture smooth electrode systems in the sub-micron scale. Such miniaturized structures can generate high electric field strengths and field gradients with low applied voltages, thus minimizing the unwanted effects of electrothermally induced motion of the suspending fluid [3]. Microelectrode structures

<sup>a</sup> email: emppu.salonen@hut.fi

<sup>b</sup> email: terama@pcu.helsinki.fi

<sup>c</sup> email: ilpo.vattulainen@hut.fi

<sup>d</sup> email: mikko.karttunen@hut.fi

employing DEP have been used, *e.g.*, in the self-assembly of micrometer-sized silicon resistors [4] and trapping of conducting nanoparticles [5,6], as well as alignment and assembly of metallic nanowires [7,8] and carbon nanotubes [9,10]. The precision obtained in these studies and the fact that many particles can be positioned in the electrode systems in a parallel fashion show that DEP is a very promising tool for the assembly of nanoelectronics devices on a larger scale (for recent reviews on the use of DEP in nanotechnology, see Refs. [11,12]). Since DEP is a non-invasive and non-destructive technique, it has also been used to manipulate biologically relevant microparticles in various applications [13,14,15,16,17,18,19,20].

In comparison to standard electrophoresis (*i.e.*, particle motion due to the coupling between an applied electric field and a non-zero net charge), DEP has the disadvantage that the polarization forces involved are typically quite weak. In general, efficient particle manipulation in microelectrode systems requires balancing DEP against other forces present, such as viscous, buoyancy, and electrohydrodynamic forces [3]. Clever experimental setups have indeed been devised to trap particles of the order of only a few nm in diameter [5,6]. But while many of the hindrances can be overcome with appropriate choices for suspending media and electric field configurations, a fundamental limit on the precision and efficiency of DEP manipulation is set by the thermal motion of the particles. For the case of stable particle trapping over long periods in time, the DEP force clearly has to be much stronger than the thermal noise from the particle-solvent interactions. To this end, reasonable criteria of the trapping conditions for isolated particles with idealized geometries can be formulated by using simplified hydrodynamics [14,16]. However, in the event of particle aggregation the situation becomes much more complicated [21,22].

Computational modeling has previously been used to study diverse electrokinetic phenomena, such as electrophoresis [23,24], overcharging and like-charge attraction [25,26,27], and structure formation in electrorheological fluids [28,29]. It is then natural to ask whether information on DEP motion of nanoparticles could be obtained from dynamic computer simulations employing simplified, but still physically sound models for particles and their interactions. The motion of nanoscopic particles and particle aggregates in electrode systems of realistic dimensions is essentially a multi-scale problem, with important processes taking place at times ranging from picoseconds (dynamic processes on the molecular scale) to microseconds (larger aggregate formation), and all the way to seconds (particle concentration in specific parts of the device). At present there exists a variety of methods to tackle multi-scale problems at different levels of accuracy [30,31,32,33].

As the initial step to computational modeling of DEP, in this article we present, to our knowledge, the first molecular dynamics (MD) simulations of dielectrophoresis. The goal of the present work is to model the DEP of a single colloidal particle at varying combinations of temperature and applied electric field strength. We verify that the model exhibits linear drift velocity to DEP force relation and further study the

particle DEP mobility and the temperature dependence of the motion.

This article is organized as follows. In Section 2, we will outline in detail and validate the nanoparticle DEP model used in the present work, and further examine the extent of finite-size effects in our model system. Section 3 then comprises the simulation results on the single-particle DEP transport. Section 4 closes the article with the concluding remarks.

## 2 Simulation method

### 2.1 General features of the model

We have used classical MD simulations to model the dielectrophoresis of a single charge-neutral colloidal particle in a non-conducting solvent. As a generic model for a polarizable particle we used a system consisting of a large sphere, carrying a charge  $q_{\text{mac}}$ , on which  $N_{\text{mic}}$  small particles with a charge  $q_{\text{mic}}$  were electrostatically bound (see Sec. 2.2). In the remainder of the text, we adopt the following terminology: the large sphere will be called *macroion*, and the small bound particles *microions*. The macroion-microion complex will be called *colloidal particle* or simply *colloid*. As the solvent particles are smaller than the colloid in linear dimension only by an order of magnitude, the colloid can be viewed as a nanoparticle immersed in a molecular solvent.

For a proper description of colloid-solvent interactions under non-equilibrium conditions, the suspending medium in which the colloid was immersed was simulated with explicit neutral particles. Excluded volume interactions between all particle types were modeled using a truncated and shifted 12-6 Lennard-Jones potential (also called the WCA potential) [34]. In order to take into account the size of the macroion, an additional hard-core radius  $r_0$  was included in the denominator of the repulsive and attractive power terms [35],

$$\Phi_{\text{WCA}} = 4\varepsilon \left[ \left( \frac{\sigma}{r_{ij} - r_0} \right)^{12} - \left( \frac{\sigma}{r_{ij} - r_0} \right)^6 \right] + \varepsilon, \quad (3)$$

where  $r_{ij} = |\mathbf{r}_j - \mathbf{r}_i|$  is the center-to-center distance between the interacting particles  $i$  and  $j$  ( $\mathbf{r}_i$  being the position vector of particle  $i$ ). The cutoff distance of the potential was  $r_0 + 2^{1/6}\sigma$ , with  $r_0 = 4.5\sigma$  for interaction pairs involving the macroion and  $r_0 = 0$  otherwise. The characteristic parameters  $\sigma$  and  $\varepsilon$  of the potential were chosen as the basic units of length and energy, respectively. With  $m$  further designating the unit of mass, the unit of time is then defined as  $\tau = \sigma\sqrt{m/\varepsilon}$ .

The simulation cell was cubic with periodic boundary conditions and a side length  $L_0 = 35\sigma$ . The solvent particles and microions were assigned a mass  $1m$  and the solvent number density was chosen as  $\rho_s = 0.3 \sigma^{-3}$ . For the macroion, the mass was chosen to correspond to the mass of bulk solvent equal to its volume, giving a value of  $155m$ . Suitable estimates for effective particle sizes could be obtained from the distances of closest approach between different particles at temperature  $T$ , using the relation  $\Phi_{\text{WCA}} = k_B T$ . Our choice of  $r_0$  then gave effective particle radii roughly  $5\sigma$  for the macroions and  $\sigma/2$  for the microions and solvent particles. Although particle

sizes defined this way depend on the system temperature, the steepness of the WCA potential slope ensured that the effective particle radii did not vary significantly in the temperature range used in this study.

## 2.2 Electrostatic interactions

The electrostatic interactions between the ions were calculated directly from Coulomb's law. The energy associated with the interaction of particles  $i$  and  $j$  was then given by

$$V_c = \frac{q_i q_j}{4\pi\epsilon_0\epsilon_r r_{ij}}, \quad (4)$$

where  $q_i$  is the charge of particle  $i$ ,  $\epsilon_0$  is the vacuum permittivity, and  $\epsilon_r$  the relative permittivity of the medium. To ensure that the microions stay bound to the macroion surface we chose the regime of strong Coulomb coupling by setting  $(4\pi\epsilon_0\epsilon_r)^{-1} = 56 \text{ e}\sigma/e^2$ , independent of temperature and constant in the entire simulation cell. We did not employ any type of lattice summation or multipole methods as this would be problematic due to the non-uniformity of the external electric field (see Sec. 2.3).

The charge  $q_{\text{mac}} = -20e$ , where  $e$  is the elementary charge, was assigned to the interaction center of the macroion. To prevent an electrophoretic component in the external electric field-induced motion, overall charge neutrality was imposed on the macroion-microion system,  $q_{\text{mac}} + N_{\text{mic}}q_{\text{mic}} = 0$ . The number and charge of the microions were then chosen as  $N_{\text{mic}} = 10$  and  $q_{\text{mic}} = +2e$ , respectively.

At a first glance, the choice of spatially uniform value of  $\epsilon_r$  may seem controversial, as the magnitude and direction of the DEP force generally result from the mismatch of the complex permittivities of the manipulated particles and the suspending medium. A purely practical reason for this simplification is the fact that taking into account the induced surface charges of polarization (image charges) on the macroion [36] is computationally extremely intensive, making dynamic simulations, such as the ones presented here, dramatically more time-consuming. However, considering the picture of a single nanoparticle in solution, it is not even meaningful to talk about its permittivity. With our generic macroion-microion system, the polarization of the colloid originates simply from the redistribution of the microions on the macroion surface.

## 2.3 External field

For the modeling of DEP, it is preferable to use an electric field geometry which is simple to realize and has a large field gradient in order to produce appreciable dielectrophoretic motion. In this work we have used a spherically symmetric DC electric field,

$$E(R) = E_0 \left( \frac{R_0}{R} \right)^2 \mathbf{e}_R, \quad (5)$$

where  $E_0$  is the electric field strength at the initial radial position  $R_0$  of the colloid, and  $\mathbf{e}_R$  is the radial unit vector. As the colloid moves in the field,  $R_0$  further determines the characteristic length over which the field strength changes

appreciably. This type of an electric field geometry is a good approximation for many experimental DEP setups [12], and was thus a reasonable choice for a model system. The DEP force arising from the non-uniformity of the field is

$$\mathbf{F}_{\text{DEP}} = -2\alpha_p \frac{E_0^2}{R_0} \left( \frac{R_0}{R} \right)^5 \mathbf{e}_R, \quad (6)$$

as results from Eq. (2). Since our model colloid is always more polarizable than the surrounding medium, the simulations corresponded to the case of positive DEP. For all the simulations presented in this article we used  $R_0 = 1500\sigma$ .

The electric field strength affecting a charged particle was calculated by using an additional coordinate system, with the origin set at the force center of the electric field. The vector  $\mathbf{R}$  was used to denote the position of the center of the microscopic simulation cell in the electric field coordinates. The position of a charged particle  $i$  was then  $\mathbf{r}'_i = \mathbf{R} + \mathbf{r}_i$ . (In the following, all coordinates marked with prime will refer to the electric field frame of reference.) We emphasize that the only effect of assigning the additional electric field coordinates for the charged particles was to take into account the spatial dependence of the electric field and its gradient. During the course of the simulations the vector  $\mathbf{R}$  was updated, and hence all  $\mathbf{r}'_i$  as well, according to the colloid displacements in the simulation cell (see below in Sec. 2.4).

In the absence of an external electric field the microions are evenly distributed on the surface of the macroion due to their mutual electrostatic repulsions. When an external field is applied, polarization of the system is obtained with the redistribution of the microions. In order to calculate the DEP force affecting the colloidal particle, its polarizability  $\alpha_p$  needed to be determined. This was done by calculating the induced dipole moment of the particle,  $\mathbf{p} = \sum_i q_i \mathbf{r}_i$ , where the summation is carried out over the ions, in the following way. The colloid was put under a selected electric field strength and the microions were allowed to freely redistribute themselves on the macroion surface. The total kinetic energy of the system was very slowly quenched to zero, resulting in a minimum energy state of the polarized colloid. Note that this type of MD energy minimization cannot rigorously guarantee that the obtained ion configuration is the true global energy minimum state of the system [27]. However, several independent energy minimization simulations showed only negligible differences in the total energy and thus the obtained values were assumed to lie very close to the true energy minimum.

As expected, the dipole moment of the macroion-microion system was observed to be linearly proportional to the electric field strength in a wide range of  $E_0$ . Deviations from the linearity occurred at very low field strengths due to microion-microion electrostatic correlations and at extremely high field strengths (above  $17 \text{ e}/e\sigma$ , which is nearly half the electric field strength due to the macroion bare charge at a distance of  $r_0 + \sigma$ ), as the microions were stripped from the macroion surface. A linear fit to the data gave the colloid a total polarizability  $\alpha_p = 4.94 \pm 0.16 \text{ e}^2\sigma^2/\epsilon$ . Comparing the DEP forces calculated with fit value of  $\alpha_p$  and Eq. (2) to the ones obtained directly from the simulations showed excellent agreement, thus validating the dipole approximation.

## 2.4 DEP simulations

The DEP simulations were carried out as follows. The polarized colloid, in its minimum energy state, was set at the center of the simulation cell and the remaining free volume was filled with randomly distributed solvent particles. In order to avoid strong repulsion forces due to excluded volume overlaps, it was ensured that all interparticle distances were larger than the WCA potential cutoff distance  $r_0 + 2^{1/6}\sigma$ . The system was then thermalized for  $85\tau$  at a selected temperature ( $T = 0.03 - 2.4 \varepsilon/k_B$ ) by coupling all the particles to the thermostat by Berendsen *et al.* [37] with a coupling time constant of  $0.14\tau$ .

The range of temperatures used in this study may sound broad in view of experiments. However, just like the electric field strength in our model is a measure of the DEP force, the temperature, in turn, is simply a measure of the random thermal forces and friction affecting the colloid. Note that since there were no attractive forces between the solvent particles and, on the other hand, the solvent density was much lower than required for hard-sphere crystallization of entropic origin, the solvent remained in a fluid state even at the lowest simulation temperatures.

After thermalization the thermostat coupling was retained only within a distance of  $1\sigma$  from the cell borders for the rest of the simulation. The border scaling was maintained in order to dissipate the heat produced from the work done by the electric field on the colloid, without affecting its DEP motion. A somewhat similar thermostat coupling scheme was also used by Tanaka and Grosberg in their simulations of nanoparticle electrophoresis [23]. In those studies it was reported that the thermostat at the cell borders serves only a minor purpose, as the amount of Joule heat produced during the simulations was very small. Our test simulations without the cell border thermostat also showed only negligible increases in the temperature. We nevertheless retained the border thermostat in the DEP simulations to dissipate any excess heat in the system.

The equations of motion were integrated using the velocity Verlet algorithm [38]. For proper energy conservation, integration time steps between  $0.002\tau$  and  $0.004\tau$ , depending on the system temperature, were used. The total simulation length, including the system thermalization time, was  $5785\tau$ . During the simulations the colloid, driven by the DEP force, could move distances corresponding up to a few simulation cell side lengths (see below in Sec. 2.5). In order to avoid artifacts due to the direct calculation of the electrostatic interactions and the colloid entering the thermal scaling region at the simulation cell borders, after each time step the origin of the simulation cell was set at the interaction center of the macroion. In practice, this means that the macroion itself was not displaced in the simulation cell, but the positions of all the microions and solvent particles were shifted instead. The position of the center of the simulation cell in the electric field coordinates,  $\mathbf{R}$ , was also shifted according to the macroion motion, as the electric field strength and its gradient changed with the colloid displacements.

For each combination of electric field strength and temperature, a total of 20 – 80 simulations were carried out in order to obtain good statistics. Larger numbers of simulations were required at higher temperatures due to thermal noise.

Although the simulations were carried out in the regime of strong Coulomb coupling (cf. Sec. 2.2), it is still valid to ask whether the microions could be stripped from the macroion surface by random collisions with the solvent particles. In that case the colloid mobility would be enhanced due to an electrophoretic component, as the particle would possess a non-zero net charge. We determined the minimum microion binding energy for the case of the highest field strength,  $E_0 = 2.70 \varepsilon/e\sigma$ , while the colloidal particle was held fixed at its initial position in the electric field. This analysis showed that even at the highest temperature used in the simulations,  $T = 2.4 \varepsilon/k_B$ , the ratio of the minimum microion electrostatic binding energy to the thermal energy  $k_B T$  was roughly 24. Hence, the macroion-microion system could be considered stable in view of collisions with the solvent particles. All the DEP simulations were further checked for possible microion detachments, but no such events were found.

If the electric field-induced colloid motion in the simulations was truly due to DEP, similar deterministic motion should be obtained regardless of the actual polarity of the electric field. However, if the direction of the colloid motion would be reversed by reversing the field polarity, the motion would be in fact due to electrophoresis. To make the final validation that the model presented here really produces DEP motion of the colloidal particle, 10 independent test simulations were carried out with both positive and negative field polarities and  $|E_0| = 0.96 \varepsilon/e\sigma$ . In order to facilitate the comparison, the solvent thermal noise affecting the colloid was minimized by selecting a very low temperature,  $T = 0.03 \varepsilon/k_B$ . The simulations were otherwise identical in the initial conditions, except that for the case of negative field polarity, the microion configurations on the macroion were rotated half a turn with respect to the radial direction. Thus, for both field polarities the colloid was close to their minimum energy state, and delayed coupling of the colloid to the electric field due to microion distribution relaxations did not hinder comparison between the two series of simulations.

In all the cases, regardless of the field polarity, the colloid moved in the direction of  $\nabla E^2$ , as was expected for positive DEP. The average colloid radial displacements for the positive and negative field polarities were  $(-14.0 \pm 2.5)\sigma$  and  $(-12.5 \pm 2.5)\sigma$ , respectively. Considering the number of test simulations carried out, it can be stated that the agreement is very good.

## 2.5 Finite-size effects

Before proceeding to the actual DEP simulations, the extent of finite-size effects in our model should be discussed. Since in general hydrodynamic effects, mediated by the solvent, are long-ranged [24,39], regardless of the simulation cell size used there always remains some contribution from interactions between the colloid and its periodic images. This imposes restrictions on the minimum size of the solvent shell used in the modeling that in principle need to be resolved for each specific systems.

Probably the best point of comparison in the literature for our model system is the one used by Tanaka and Grosberg in their MD simulations of nanoparticle electrophoresis [23]. The authors used a similar WCA solvent and also the same

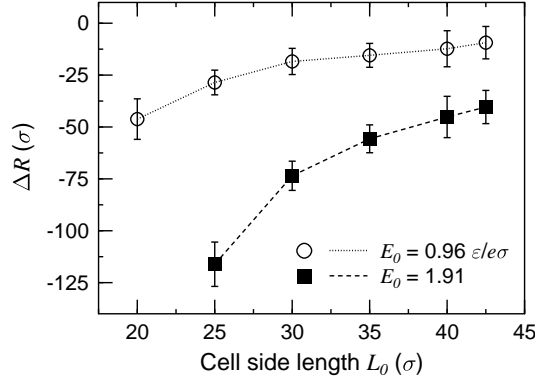


**Fig. 1.** Colloid average radial displacements as a function of the simulation cell side length  $L_0$ . The error bars in the figure correspond to the standard deviations of the radial displacements.

solvent number density as in our model. The colloid radius in their simulations varied between  $3\sigma$  and  $7\sigma$ . From tests on the simulation cell size dependence the authors concluded that a value of  $L_0 = 20\sigma$  was sufficient to yield statistically reliable electrophoretic drift velocities. The actual electrophoresis simulations were then carried out with  $L_0 = 32\sigma$ . An important difference between our simulation system and the one used by Tanaka and Grosberg is that the latter included co- and counterions in the solvent, which the authors stated to shield hydrodynamic interactions. It should be also noted that in principle the thermostat coupling at the simulation cell borders we have used could affect the colloid hydrodynamic interactions. However, as the thermostat coupling was quite weak, this effect should be very small or even negligible. This is corroborated by the tests of Tanaka and Grosberg on the cell border thermostat and nanoparticle electrophoretic drift velocities [23].

We tested several simulation cell sizes in order to find a value of  $L_0$  small enough for good computational efficiency, but still large enough to result in reasonably small finite-size effects. As the measure for an adequate value of  $L_0$  we used the colloid average radial displacements,  $\langle \Delta R \rangle$ , in reference to the electric field coordinates, at  $E_0 = 0.96$  and  $1.91 \varepsilon/e\sigma$ . Like in the tests of opposite electric field polarities (Sec. 2.4), we used a temperature of  $0.03 \varepsilon/k_B$  to minimize statistical fluctuations. Figure 1 shows the results from several tests employing simulation cell side lengths between  $20\sigma$  and  $42.5\sigma$  with 2239 and 22728 solvent particles, respectively.

For both  $E_0$  used the absolute values of the colloid average radial displacements  $\langle \Delta R \rangle$  increased with decreasing  $L_0$ . This is in contrast with the well-known enhancement of hydrodynamic friction, proportional to  $L_0^{-1}$  [24, 39]. However, standard hydrodynamic considerations assume an incompressible fluid, which is not the case with our system. In the simulations of nanoparticle electrophoresis, Tanaka and Grosberg also observed [23] increased particle drift velocities for smaller values of  $L_0$ . Although in their case the solvent size dependence of the particle velocity was not smooth as observed here, the effect could be due to the general properties of the low-density WCA solvent.

A measure of the relative efficiencies of momentum and mass transport in a fluid at equilibrium is given by the Schmidt

number,

$$Sc = \frac{\eta}{\rho_m D_s}, \quad (7)$$

where  $\eta$ ,  $\rho_m$  and  $D_s$  are the fluid shear viscosity, mass density, and self-diffusion coefficient, respectively. In real liquids  $Sc$  is typically of the order of  $10^3$  and thus momentum propagates much faster than mass in the medium. However, for our model solvent, simple estimates based on the theory of hard sphere fluids [40] result in values of  $Sc \approx 3 - 5$  (depending on the temperature). This suggests that the apparent friction on the colloid under non-equilibrium conditions is strongly connected to the number of solvent particles and hence,  $L_0$ . Considering the fact that momentum is not conserved in our DEP simulations (due to the work done by the electric field on the colloidal particle and also, to some extent, due to the temperature scaling only at the simulation cell borders), the exact coupling between the solvent flow field and the colloid dynamics becomes hard to assess with analytical means.

Based on the tests, we selected a value of  $L_0 = 35\sigma$ , with 12687 solvent particles, for the actual DEP simulations. This value of  $L_0$  still seems to produce larger radial displacements than would be obtained for a system with a much higher number of solvent particles. However, since all the simulations were carried out with the same system size, and our purpose is to provide qualitative rather than quantitative insight on DEP, we do not expect finite-size effects to affect the conclusions of the present work.

### 3 Results

In this Section we present the analysis of the DEP simulations. In all the cases the initial position of the colloidal particle was set at a distance  $R_0 = 1500\sigma$  on the  $x'$ -axis. Hence, at the start of the simulations the DEP force drove the colloid in the negative  $x'$ -direction, while motion in the  $y'z'$ -plane was perpendicular to the DEP force. The DEP force affecting the colloid was varied using four different electric field strengths with  $E_0 = 0.96, 1.35, 1.91$ , and  $2.70 \varepsilon/e\sigma$ . Since in our electric field geometry  $F_{\text{DEP}} \propto E_0^2$ , the ratios of the initial DEP forces were approximately 1:2:4:8. The simulations were carried out at temperatures between  $0.03$  and  $2.4 \varepsilon/k_B$ . The margins of error for the quantities presented below are estimated from the error of the mean.

In view of DEP manipulation in the nanoscale, it is instructive to compare the DEP force to the thermal noise of the surrounding solvent. For the latter, a characteristic force is given by the ratio of the thermal energy to the linear size of the particle in question,

$$F_{\text{thermal}} = \frac{k_B T}{2a_0}, \quad (8)$$

where in our case  $a_0 \approx r_0 + \sigma/2$  is the radius of the spherical macroion. A dimensionless parameter describing the ratio of the thermal noise to the DEP force, is then defined as

$$\Theta_{\text{DEP}} = \frac{F_{\text{thermal}}}{F_{\text{DEP}}} = \frac{k_B T}{\alpha_n a_0 |\nabla E^2|}. \quad (9)$$

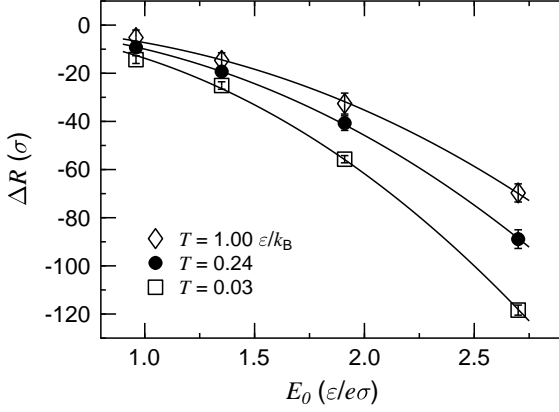


**Fig. 2.** Average colloid radial displacements, as a function of  $E_0$ , at the end of the simulations for three different temperatures. The solid lines are the results of the regression analysis between the radial displacements and the spatially variant DEP force (see text).

At small values of  $\Theta_{\text{DEP}}$  the DEP force dominates over the thermal motion of the colloid, whereas at large values the colloid motion becomes increasingly random. In the range of electric field strengths and temperatures used in this study the values of  $\Theta_{\text{DEP}}$  varied nearly three orders of magnitude, from 0.07 to 40. However, there is an important point to note here. As the DEP force is strongly dependent on the radial position in the electric field ( $F_{\text{DEP}} \propto R^{-5}$ ), the value of  $\Theta_{\text{DEP}}$  is not fixed. For example, a colloid that has traversed a distance of  $100\sigma$  radially inward in the electric field experiences a DEP force that is 41% larger than the force at its initial position,  $R_0 = 1500\sigma$ . This further entails that at sufficiently long times particle distributions in the radial direction become asymmetric with a negative value of skewness.

It can be questioned whether the DEP force originating from the polarization of the macroion-microion complex is the same at all temperatures. As the solvent particles collided with the microions, the dipole moment of the polarized colloid fluctuated around the value corresponding to the minimum energy state. However, even at the highest temperatures used, these deviations were not strong enough to divert the mean orientation of the dipole moment from the one induced by the electric field. For all cases the characteristic fluctuation time of the dipole moment was very short in comparison with the length of the simulation. It was then plausible to take the average force affecting the colloid as the one given by Eq. (6). Test simulations with a spatially dependent, but non-fluctuating, artificial force affecting the colloid showed similar radial displacements as in the DEP case (data not shown), further corroborating the approximation.

### 3.1 DEP at constant temperature

The main results of our simulations were the colloid radial displacements in the electric field, *i.e.*, motion in the direction parallel to the DEP force. We first consider series of simulations where the system temperature was kept constant and  $E_0$  was varied. The average radial displacements of the colloid,  $\langle \Delta R \rangle$ , for three different temperatures are shown in Fig. 2. The

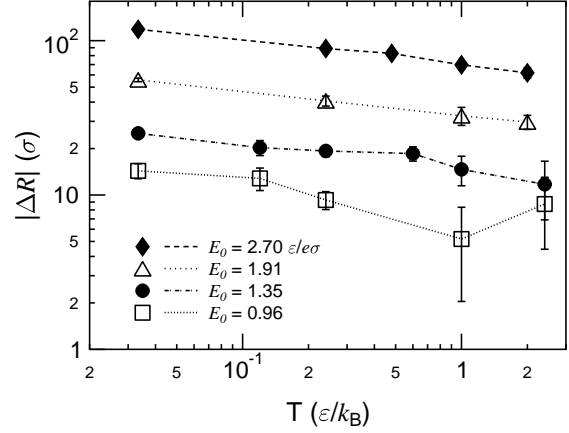


**Fig. 3.** Absolute values of the average colloid radial displacements for the different values of  $E_0$  as a function of temperature.

increase of the radial displacements with the increase of  $E_0$  and the decrease of  $T$  is evident.

The ratios of the DEP drift velocities,  $\langle v_{\text{DEP}} \rangle = \langle \Delta R \rangle / \Delta t$ , and the colloid thermal velocities at the respective temperatures were of the order of 0.01 – 1. At these low values the DEP drift velocities should be linearly proportional to the DEP force. The average radial displacement over a time interval  $\Delta t$  is then

$$\langle \Delta R \rangle = \frac{F_{\text{DEP}}}{\xi} \Delta t, \quad (10)$$

where  $\xi$  is the friction factor of the solvent. Regression analysis between the particle radial displacements and the DEP force,  $\langle \Delta R \rangle \propto [F_{\text{DEP}}]^\nu$ , justified this assumption. However, for an accurate analysis it was required to taken into account the fact that the particle in our simulation is under spatially variant force field: As the radial position of the colloid changes, so does the magnitude of the electric field and its gradient. Hence, the radial displacements were compared to the average DEP force experienced by the colloid, as calculated from the particle trajectories. The resulting values of  $\nu$  were, within statistical errors, equal to unity (see Fig. 2).

On the other hand, simply taking the value of the DEP force at the start of the simulation,  $F_{\text{DEP}}(R_0)$ , resulted in values of  $\nu$  slightly higher than one.

### 3.2 Temperature dependence and DEP mobility

The data in Fig. 2 indicate that the dependence of the DEP displacements on temperature is quite weak. We now analyze this observation in more detail.

Figure 3 shows the colloid radial displacements, as a function of temperature, for four series of simulations corresponding to different values of  $E_0$ . Note that the data presented are the absolute values of the radial displacements (in order to make the full logarithmic plot) but all the real values of the displacements were in fact negative, *i.e.*, in the direction of the DEP force. The data show a clear power law behavior, although for the two lower values of  $E_0$ , at the highest temperatures, the diffusive motion of the colloid contributes significantly to the

scatter in the DEP displacements. This is characterized by high values of the parameter  $\Theta_{\text{DEP}} \approx 8 - 40$ .

As the linear response was shown to hold above, a straightforward assumption is that the friction factor  $\xi$  should be linearly proportional to the solvent shear viscosity  $\eta$ . An estimate for the temperature dependence of our solvent viscosity can be obtained from the well-known Enskog expression for hard-sphere fluids [40]. It has been shown to give good agreement with MD calculations employing low-density WCA potential solvents [41] (such as the one in our case) and further even qualitatively describe much more complex systems where one would not necessarily expect the hard-sphere approximation to hold [42]. For the Enskog viscosity the temperature dependence is  $\eta \propto \sqrt{T}$ . Although one could assume even a qualitative agreement with our low-density WCA solvent friction and the one given by the Enskog theory, this is clearly not the case (cf. Fig. 3). What is then the reason for the scaling of the DEP displacements shown in Fig. 3?

Analogous to the case of electrophoresis under uniform  $\mathbf{E}$ , it is possible to define DEP mobility [17],  $\mu_{\text{DEP}}$ , that yields the particle drift velocity due to the electric field,

$$\langle \mathbf{v}_{\text{DEP}} \rangle = \mu_{\text{DEP}} \nabla E^2. \quad (11)$$

Combining Eqs. (2), (10), and (11) yields the general form

$$\mu_{\text{DEP}} = \frac{\alpha_p}{2\xi}. \quad (12)$$

However, care should be taken here. As mentioned above, contrary to the case where true steady-state condition can be attained, the value of  $\nabla E^2$  changes constantly with particle motion. Calculating  $\mu_{\text{DEP}}$  from large particle displacements and simply using the initial value of  $\nabla E^2$  can lead to significant errors.

Using Eq. (11) we calculated the colloid mobilities from the particle trajectories and the average values of  $\nabla E^2$ , over a given time interval  $\Delta t$  from the beginning of the simulations. The results of these calculations for two different temperatures are shown in Figs. 4 and 5. For clarity, we only show the results for two different values of  $E_0$  in each plot. The data for all  $E_0$ , at each respective temperature, were consistent with each other. Also note that for lower values of  $E_0$  the data are somewhat noisier due to the stronger diffusive motion.

The main observation here is that the values of  $\mu_{\text{DEP}}$ , and hence the values of the friction factor  $\xi$  (cf. Eq. (11)), vary with time. Thus, there is a clear coupling of the non-equilibrium motion of the colloid to the solvent velocity field. Although a thorough analysis of this effect is challenging, it is not unreasonable to assume that the characteristic time scale for the evolution of the non-equilibrium transport (with a constantly changing friction factor) would be different at different temperatures. Indeed, a further study of the *apparent* temperature dependence of the DEP displacements (such as shown in Fig. 3 for the final radial displacements in the simulations) revealed that while power law expressions could be fitted to the displacement data at different points in time, the resulting exponents were not constant. We do not want to put too much emphasis on the actual values of these data, as we were unable to find a satisfactory theoretical way of interpreting them.

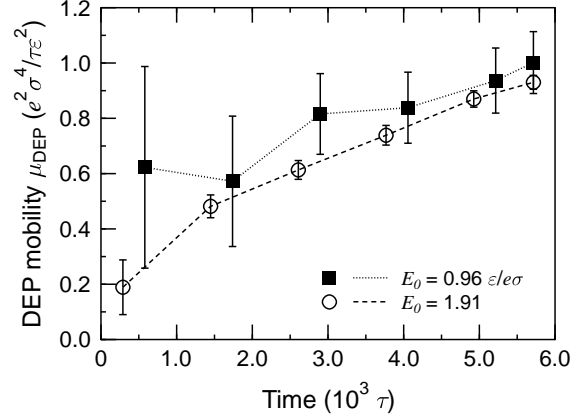


**Fig. 4.** Colloid mobility  $\mu_{\text{DEP}}$  as a function of time for  $E_0 = 0.96$  and  $1.91 \varepsilon/e\sigma$  at  $T = 0.03 \varepsilon/k_B$ .

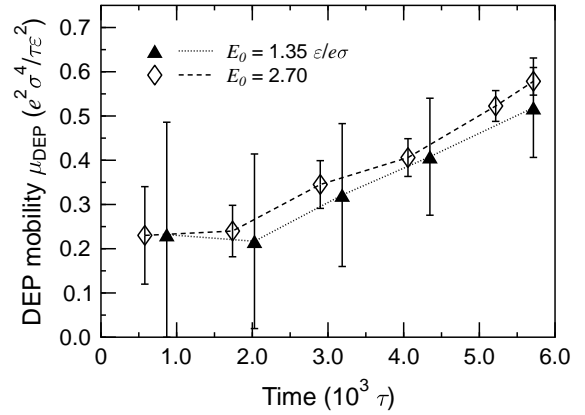


**Fig. 5.** Same as Fig. 4 but for  $E_0 = 1.35$  and  $2.70 \varepsilon/e\sigma$  at  $T = 1.0 \varepsilon/k_B$ .

### 3.3 Lateral displacements

Another interesting aspect of the spatial dependence of the colloid motion is seen by studying it in the plane perpendicular to the electric field gradient at the initial particle position, *i.e.*, in the  $y'z'$ -plane. At the beginning of the simulation the colloidal particle is directed toward the negative  $x'$ -direction by the DEP force. Deviations from this direction then affect the precision of the DEP manipulation, *i.e.*, how accurately the final position of the particles can be predetermined.

To a very good approximation the average displacements of the colloid in the  $y'$ - and  $z'$ -directions were zero for all the combinations of  $E_0$  and  $T$ . We then calculated the displacements in the  $y'z'$ -plane,  $\Delta R_{\text{lat}}$ . For comparison, we also determined the colloid tracer diffusion coefficient  $D = (3.65 \pm 0.07) \times 10^{-2} \sigma \sqrt{\varepsilon/m}$  at  $T = 1.0 \varepsilon/k_B$  in the absence of the external electric field. This was done using the Green-Kubo relation between the diffusion coefficient and the particle velocity autocorrelation function [40],

$$D = \frac{1}{3} \int_0^\infty \langle \mathbf{v}(0) \cdot \mathbf{v}(t) \rangle dt. \quad (13)$$

A total of 10 independent simulation runs were carried out with a length of  $15800\tau$  each. The integrals of the velocity

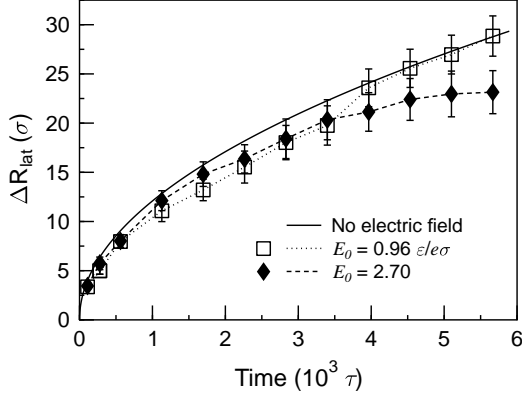


**Fig. 6.** Lateral ( $y'z'$ ) displacements  $\Delta R_{\text{lat}}$  as a function of time at  $T = 1.0 \varepsilon/k_B$ . The solid line is the prediction obtained from  $\Delta R_{\text{lat}}(t) = \sqrt{4Dt}$ .

autocorrelation functions were calculated over time periods of  $158\tau$  with a sampling interval of  $0.002\tau$  to ensure proper convergence.

A comparison between the average lateral displacements for the two extreme cases  $E_0 = 0.96$  and  $2.70 \varepsilon/e\sigma$ , and the root-mean-square displacement predicted by the relation  $\Delta R_{\text{lat}} = \sqrt{4Dt}$  is shown in Fig. 6. In the case of  $E_0 = 0.96 \varepsilon/e\sigma$ , for which  $\langle \Delta R \rangle$  was small, the colloid average lateral displacement is in a good agreement with the zero-field diffusion prediction. However, at  $E_0 = 2.70 \varepsilon/e\sigma$  a clear difference is seen. This indicates that with decreasing radial position in the electric field, the high electric field gradient produces a steering effect on the colloid. Deviations from motion along the  $x'$ -axis result in DEP force components also in the  $y'$ - and  $z'$ -directions, and the assumption of independent motion in the  $x'$ -direction and, on the other hand, in the  $y'z'$ -plane breaks down. It is also possible that the coupling of the particle motion to the solvent velocity field suppresses the lateral motion up to some degree.

A general relation between the solvent friction and diffusion coefficient of a particle is given by the Einstein relation

$$D = \frac{k_B T}{\xi}, \quad (14)$$

regardless of the actual mechanism causing the friction. From the simulated value of  $D$  we calculated the friction factor  $\xi = 27.4 \pm 0.5 \sqrt{\varepsilon m}/\sigma$ , corresponding to the case of zero external electric field. It is interesting to compare this value to the time-dependent  $\xi$  in the DEP simulations. Inserting the value of  $\xi$  above into Eq. (12) results in  $\mu_{\text{DEP}} = (0.090 \pm 0.003) e^2 \sigma^4 / \tau \varepsilon^2$  in equilibrium. This is comparable to the values of  $\mu_{\text{DEP}}$  in the non-equilibrium simulations only at very short times, see Fig. 5. Although not conclusive, the analysis here implies that at the beginning of the simulation the DEP mobility is very close to the value obtained by using an equilibrium friction factor. The coupling to the solvent velocity field then gradually lowers the solvent friction factor in time and the particle motion loses its equilibrium nature.

## 4 Concluding Remarks

We have carried out extensive MD simulations of a spherical nanoparticle DEP in a non-conducting solvent. This study is, to our knowledge, the first MD study of DEP and serves as a benchmark for future work employing more complex colloid, solvent, and electric field models.

The main results of our simulations were the radial displacements of the colloidal particle due to the DEP coupling. The analysis of these displacements first showed that the assumption of linear response was justified for simulation series carried out at constant temperatures. That is, the DEP drift velocities were linearly proportional to the DEP force. For an accurate analysis it was required to take into account the spatial dependence of the electric field, even at the short time scale of the present simulations.

The comparison of simulation series at different temperatures showed a weak apparent temperature dependence. We emphasize here again that the magnitude of this dependence was observed to vary with the time scale over which the particle motion was studied. Furthermore, the particle DEP mobilities, defined by Eq. (11), were observed to increase in time. This is clearly a manifestation of the non-equilibrium nature of the particle motion. The intricate coupling of the particle drifting to the solvent velocity field decreased the friction factor  $\xi$  (which is inversely proportional to the mobility). A rigorous analytical treatment of this effect is indeed challenging, and is left as a subject for future work.

Finally, the analysis of the colloid lateral displacements showed that while the DEP mobility itself was shown to be time-dependent, for the lowest value of  $E_0$  the colloid motion perpendicular to the initial direction of the DEP force could still be well predicted by an equilibrium diffusion coefficient. With increased DEP coupling, this no longer applied and the lateral motion became coupled to the DEP drifting. Intuitively, this is not surprising. However, it is an important effect in determining the precision of particle transport, and we are not aware of any direct quantification of such steering effects neither in experiments nor computational studies of DEP.

Although thermal motion of the nanoparticles sets limitations on the DEP forces required for their deterministic motion, other hampering effects such as the fluid streaming induced by local heating [3] can be suppressed with proper experimental set-ups. For these conditions simple dynamic particle simulations, such as the ones presented here, can yield valuable insight on the conditions, precision, and time scales of efficient transport and stable trapping. This is especially important with particle sizes decreasing to the nanometer range, where the direct observation of the manipulated particles and their aggregates becomes very difficult in experiments.

We would like to thank K. W. Yu for many interesting discussions. This project was supported by the Academy of Finland under project Nos. 209297 (E.S.), 202598 (E.T.), 80246 (I.V.), and 0019 (M.K.). Grants of computer time from the Finnish IT center CSC in Espoo, Finland, and the Danish Center for Scientific Computing DCSC at the University of Southern Denmark are gratefully acknowledged.

## References

1. H. A. Pohl, J. Appl. Phys. **22**, 869 (1951).
2. H. A. Pohl, J. Appl. Phys. **29**, 1182 (1958).
3. A. Ramos, H. Morgan, N. G. Green, and A. Castellanos, J. Phys. D: Appl. Phys. **31**, 2338 (1998).
4. S. W. Lee and R. Bashir, Appl. Phys. Lett. **83**, 3833 (2003).
5. A. Bezryadin, C. Dekker, and G. Schmid, Appl. Phys. Lett. **71**, 1273 (1997).
6. L. Zheng, S. Li, J. P. Brody, and P. J. Burke, Langmuir **20**, 8612 (2004).
7. P. A. Smith, C. D. Nordquist, T. N. Jackson, T. S. Mayer, B. R. Martin, J. Mbindyo, and T. E. Mallouk, Appl. Phys. Lett. **77**, 1399 (2000).
8. K. D. Hermanson, S. O. Lumsdon, J. P. Williams, E. W. Kaler, and O. D. Velev, Science **294**, 1082 (2001).
9. K. Yamamoto, S. Akita, and Y. Nakayama, J. Phys. D.: Appl. Phys. **31**, L34 (1998).
10. R. H. M. Chan, C. K. M. Fung, and W. J. Li, Nanotechnology **15**, S672 (2004).
11. M. P. Hughes, Nanotechnology **11**, 124 (2000).
12. P. J. Burke, in *Encyclopedia of Nanoscience and Nanotechnology*, edited by H. S. Nalwa (American Scientific Publishers, Stevenson Ranch, CA, 2004).
13. G. H. Markx, Y. Huang, X. Zhou, and R. Pethig, Microbiology **140**, 585 (1994).
14. M. Washizu, S. Suzuki, O. Kurosawa, T. Nishizaka, and T. Shinohara, IEEE Trans. Indust. Appl. **30**, 835 (1994).
15. F. F. Becker, X.-B. Wang, Y. Huang, R. Pethig, J. Vykoukal, and P. R. C. Gascoyne, J. Phys. D: Appl. Phys. **27**, 2659 (1994).
16. M. P. Hughes and H. Morgan, J. Phys. D.: Appl. Phys. **31**, 2205 (1998).
17. H. Morgan, M. P. Hughes, and N. G. Green, Biophys. J. **77**, 516 (1999).
18. C.-F. Chou, J. O. Tegenfeldt, O. Bakajin, S. S. Chan, E. C. Cox, N. Darnton, T. Duke, and R. H. Austin, Biophys. J. **83**, 2170 (2002).
19. Y. Huang, S. Joo, M. Duhon, M. Heller, B. Wallace, and X. Xu, Anal. Chem. **74**, 3362 (2002).
20. D. S. Gray, J. L. Tan, J. Voldman, and C. S. Chen, Biosens. Bioelectr. **19**, 1765 (2004).
21. J. P. Huang, M. Karttunen, K. W. Yu, and L. Dong, Phys. Rev. E **67**, 021403 (2003).
22. J. P. Huang, M. Karttunen, K. W. Yu, L. Dong, and G. Q. Gu, Phys. Rev. E **69**, 051402 (2004).
23. M. Tanaka and A. Y. Grosberg, Eur. Phys. J. E **7**, 371 (2002).
24. I.-C. Yeh and G. Hummer, Biophys. J. **86**, 681 (2004).
25. P. Linse and V. Lobaskin, Phys. Rev. Lett. **83**, 4208 (1999).
26. R. Messina, C. Holm, and K. Kremer, Phys. Rev. Lett. **85**, 872 (2000).
27. M. Patra, M. Patriarca, and M. Karttunen, Phys. Rev. E **67**, 031402 (2003).
28. D. J. Klingenberg, F. van Swol, and C. F. Zukovski, J. Chem. Phys. **91**, 7888 (1989).
29. R. Tao and Q. Jiang, Phys. Rev. Lett. **73**, 205 (1994).
30. A. P. Lyubartsev, M. Karttunen, I. Vattulainen, and A. Laaksonen, Soft Materials **1**, 121 (2003).
31. *Novel Methods in Soft Matter Simulations, Lecture Notes in Physics*, edited by M. Karttunen, I. Vattulainen, and A. Lukkari-nen (Springer Verlag, Berlin, 2004).
32. I. Vattulainen and M. Karttunen, in *Handbook of Theoretical and Computational Nanotechnology*, edited by M. Rieth and W. Schommers (American Scientific Publishers, Stevenson Ranch, CA, to appear in 2005).
33. T. Murtola, E. Falck, M. Patra, M. Karttunen, and I. Vattulainen, J. Chem. Phys. **121**, 9156 (2004).
34. J. D. Weeks, D. Chandler, and H. C. Andersen, J. Chem. Phys. **54**, 5237 (1971).
35. B. B. Laird and J. L. Skinner, J. Chem. Phys. **90**, 3274 (1989).
36. R. Messina, J. Chem. Phys. **117**, 11062 (2002).
37. H. J. C. Berendsen, J. P. M. Postma, W. F. van Gunsteren, A. DiNola, and J. R. Haak, J. Chem. Phys. **81**, 3684 (1984).
38. M. P. Allen and D. J. Tildesley, *Computer Simulation of Liquids* (Oxford University Press, Oxford, 1989).
39. B. Dünweg and K. Kremer, J. Chem. Phys. **99**, 6983 (1993).
40. J. P. Hansen and I. R. McDonald, *Theory of Simple Liquids*, 2nd ed. (Academic Press, San Diego, 1986).
41. M. Bishop and J. P. J. Michels, Chem. Phys. Lett. **94**, 209 (1983).
42. T. Scopigno, R. Di Leonardo, L. Comez, A. Q. R. Baron, D. Fioretto, and G. Ruocco, Phys. Rev. Lett. **94**, 155301 (2005).